Trans Indian Inst Met
https://doi.org/10.1007/s12666-023-03037-6

ORIGINAL ARTICLE

In Retrospect: Some Peculiarities Observed in the Mechanical Activation of Ground-Granulated Blast Furnace Slag and Fly Ash

Rakesh Kumar[1,2]

Received: 5 February 2023 / Accepted: 27 June 2023

Abstract The focus of this paper is on the mechanical activation of aluminosilicate wastes, namely ground-granulated blast furnace slag (GGBFS) and fly ash (FA). The subject is of relevance to the development of improved blended cements and geopolymers. The presence of large quantities of amorphous phases in these materials makes them unique and challenging from the point of view of characterisation. Interesting findings, some of which were first-time discoveries, are reviewed with emphasis on the role of the milling device (mill type, milling energy, and environment), characterisation challenges, and the manifestation of mechanically induced reactivity. The relative importance of mechanical activation vis-à-vis reaction temperature is highlighted based on calorimetric maps for the geopolymerisation of fly ash.

Keywords Ground-granulated blast furnace slags · Fly ash · Mechanical activation · Hydration · Geopolymerisation · Reactivity

1 Introduction

Mechanical activation (MA), the term coined by Adolf Smekal [1], refers to the alteration in reactivity of a substance through physicochemical changes induced by high-energy milling [2–6]. In the recent past, the applications of mechanochemistry in the processing and development of novel materials are expanding exponentially [2–9].

The book 'Mechanical activation of minerals by grinding pulverising and morphology of particles' by Juhasz and Opoczky (1991) covers extensively the early research on silicates, including cement clinker and blast furnace slag [10]. Initial studies on the mechanochemical activation of cement date back to the late 1950s [10–12]. While the use of granulated blast furnace slag started in 1865 in Germany [13] and that of fly ash at the beginning of the twentieth century [14], interest in the reactivity of these materials arose around four decades back. The Hungarian researchers (1986) attributed improvements in the hydraulic activity of ground-granulated blast furnace slag (GGBFS) to deep-seated structural changes induced during milling [15]. In controlled particle size distribution (CPSD) cement, finer grinding of clinker was used to compensate for the relatively slow reactivity of fly ash and granulated slag [16, 17]. American Concrete Institute (ACI) Special Publication (SP-114) documented (in 1989), the influence of the fineness of fly ashes on their hydraulic activity [18]. Mechanical activation of aluminosilicate wastes is used to enhance their reactivity and develop improved blended cement, that is, cement with enhanced replacement of clinker by ground-granulated blast furnace slag (GGBFS) or fly ash (FA), and geopolymers or alkali-activated materials of very high strength. Developed in the 1990s, 'Energetically modified cement (EMC)' [19] and high-performance (HP) cement [20] are typical examples in which mechanically induced reactivity of aluminosilicate wastes (e.g. glass, slag, fly ash, etc.) is commercially exploited. Geopolymers with more than 100 MPa strength have been developed using mechanically activated fly ash [21].

Supplementary Information The online version contains supplementary material available at https://doi.org/10.1007/s12666-023-03037-6.

✉ Rakesh Kumar
rakesh.nmlindia@gmail.com

[1] Indian Institute of Technology (IIT-ISM), Dhanbad 826 004, India

[2] National Metallurgical Laboratory (CSIR-NML), Jamshedpur 831 007, India

Published online: 14 July 2023

The research interest in the mechanical activation of aluminosilicate wastes has steadily increased in the last two decades or so, due to the high potential to develop improved cementitious materials. The gist of these efforts is summarised in Supplementary Table 1. The studies having diverse nature encompass a wide spectrum of aluminosilicate wastes (fly ash of different types, ferrous and nonferrous slags, tailings), additions (alkali-earth carbonates, lime/limestone), devices (vibratory mills, attrition mills, planetary mills, ball mills, etc.), milling environment (air, CO_2, water, alcohol), and reaction temperature. The majority of the research is directed towards blended cements [S1–S26][1] and geopolymers/alkali-activated materials [S27–S65]. The research (Supplementary Table 1) in general focuses on the utilisation of activated wastes and there is emphasis on structure and properties of the developed materials. Limited attention is given to the interrelationship between the milling-induced structural changes in the solid and the milling variable. An in-depth understanding of the mechanisms of mechanical activation is often lacking. Mechanical activation is also confused with fine grinding and its beneficial effect is attributed to reduction in size or increased surface area alone [S16–S19, S39, S49].

This paper is based on the research carried out at CSIR-National Metallurgical Laboratory (CSIR-NML), under the New Millennium Indian Technology Initiative (NMITLI) project on improved blended cement using mechanical activation and beyond [22–37]. The focus is on the mechanical activation of GGBFS and FA. The paper looks at some of the interesting findings in retrospect. It is divided into three parts. Firstly, a general introduction to mechanical activation is given for clarity on the terminology and variables involved [10, 38]. A broad description of GGBFS and FA follows next. Illustrative examples in the third part highlight the role of the milling variables and some open questions related to the characterisation of the activated materials. Milling-induced reactivity as manifested during the hydration of the neat slag and geopolymerisation of fly ash forms the core of the paper. This paper is apt for this festschrift honouring Prof. P.C. Kapur who contributed significantly to cement and fly ash research and mentored the NMITLI project as a member of its national steering committee.

2 Mechanical Activation

The change in the energy of a dispersed system (ΔE) which includes contributions from changes in lattice energy (ΔE_u) and surface energy (Δ(specific surface energy (e_γ) x surface area (a_s)) is related with grinding energy (grinding work (W_z) x grinding efficiency (n_z)) [10, 38]

$$\Delta E = \Delta E_u - \Delta(e_\gamma a_s) = n_z W_z \tag{1}$$

Based on Eq. 1, three broad stages of grinding can be identified [10]:

Stage—I: mechanical dispersion or coarse grinding, where on grinding only the specific surface is altered with no change in the structure of surface and bulk solid; Eq. 1 gets simplified to

$$\Delta E = -e_\gamma \Delta a_s = n_z W_z \text{ (Rittinger's equation)} \tag{2}$$

Stage—II: surface activation or fine grinding, both the specific surface and the specific surface free energy change but no structural change in bulk occur, that is

$$\Delta E = -\Delta(e_\gamma a_s) = n_z W_z \text{ (Smekal equation)} \tag{3}$$

Stage—III: mechanical/mechanochemical activation, may involve alteration in the surface and bulk structure and the general Eq. 1 holds.

As depicted in Fig. 1, the physicochemical changes induced during grinding are mill and material specific [2–5, 10]. Depending on stress mechanisms (shear + impact, impact, and shear), a wide spectrum of milling devices are available. The transfer of energy between media and material has a pulsed character and is dependent on energy intensity (e.g. media size, density, and motion), the contact area between material and media (size and relative amount of media and material), milling time, and milling environment. Depending on the magnitude of the stress field created by the absorbed energy and its relaxation pathways, the material may experience heating, grinding (surface effects), and mechanical activation (bulk effects) (Fig. 2). The reactivity of the solid is influenced by changes in surface area and surface state (adsorption, repeated welding of interfaces, and fracture leading to dynamic creation of fresh surfaces), stresses and defects induced in the solid structure, surface microtopography, phase transformations, localised and overall thermal effects, etc. [2–6, 8, 10, 39–43]. The milling environment (air/gas, wet/dry, presence of surfactant) plays an important role and alters the process of grinding and mechanical activation [2, 4, 5, 10]. The role of a fluid phase during mechanical activation is reviewed in recent papers [2, 5]. It has been reported that transient hydrothermal conditions may be created during milling [2]. The CO_2 atmosphere and the presence of alkali-earth carbonates during the milling of silicates has been shown to promote mechanical activation [S34, S50–S52].

[1] The suffix S with reference number means that it refers to the list given with supplementary Table 1.

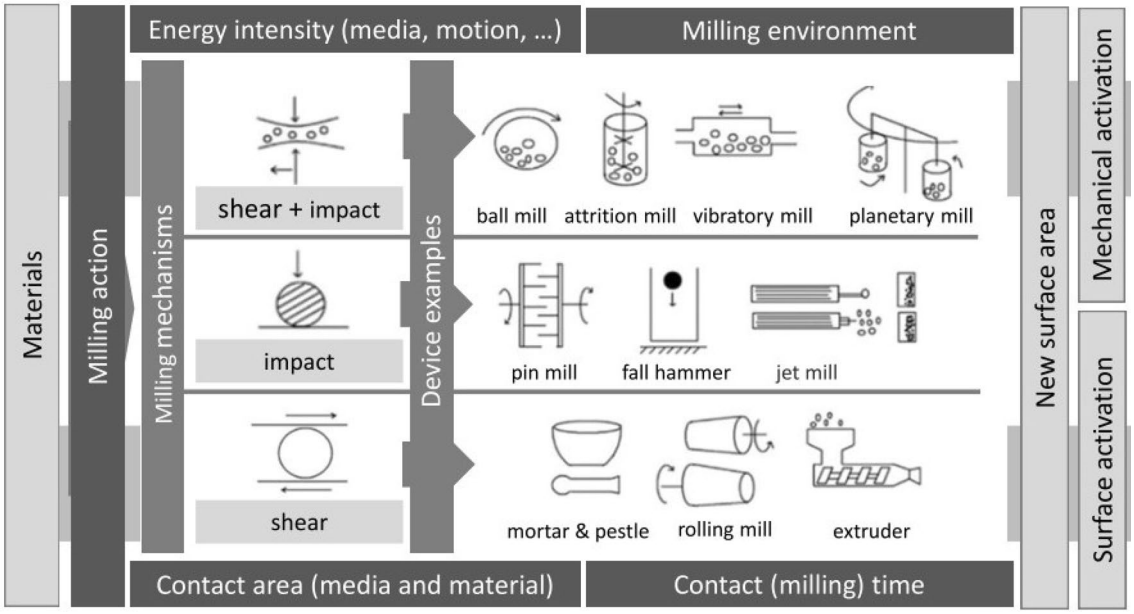

Fig. 1 The process of milling and milling-induced physicochemical changes in a solid material. The figure highlights the wide spectrum of available milling devices based on the different milling mechanisms (shear + impact, impact, and shear) and the milling conditions affecting the changes that include energy intensity, the contact area between media and feed material, milling time (or the number of hits), and milling environment (adapted from reference [4, 5, 39])

3 Ground-Granulated Blast Furnace Slag and Fly Ash

Ground-granulated blast furnace slag (GGBFS) and fly ash (FA) are the by-products of iron-making in blast furnaces and coal-fired thermal power plants, respectively. These two aluminosilicate materials differ in terms of their chemistry and mineralogical makeup. The composition regimes of fly ash and GGBFS are shown in the SiO_2–Al_2O_3–CaO ternary diagram (Fig. 3) [44]. For comparison, the location of cement clinker is also included in the diagram. The CaO content of these materials follows the order: clinker > BF slag > fly ash.

The major oxides such as SiO_2 (27–42 mass %), CaO (30–50%), Al_2O_3 (5–33%), and MgO (0–21%) constitute the bulk of the BF slag [11, 31]. The glass content (amorphous or vitreous phase) content of GGBFS may exceed 90%. A GGBFS sample from one of the integrated steel plants in the state of Chhattisgarh (India) was found to contain (in mass %) 33.1 SiO_2, 21.6 Al_2O_3, 0.87 Fe_2O_3, 33.0 CaO, and 8.85 MgO. The glass content of the slag was found to be 94% and the only detectable crystalline phase was gehlenite (2CaO. Al_2O_3. SiO_2 or C_2AS) [31].

Depending on the CaO content, as per ASTM C 618 [45], fly ash may be classified as Class F (low lime, < 5% CaO) and Class C (high lime, > 15% CaO) fly ash. Almost all Indian fly ash comes under the category of Class F and SiO_2–Al_2O_3–Fe_2O_3 content of the fly ash may exceed 90%. The glass content of Class F fly ash varies between 30 and 50%, and mullite ($Al_2Si_2O_8$), quartz (SiO_2), and magnetite (Fe_3O_4) may be present as crystalline phases [46]. As an illustration, the typical composition (in mass %) of fly ash used in a cement plant in the state of Chhattisgarh (India) is as follows: SiO_2—60.5, Al_2O_3—28.2, Fe_2O_3—4.5, CaO—1.7, MgO—0.47, Na_2O—0.14, K_2O—1.4, loss on ignition (LOI)—1.6. The glass content, as determined by petrographic analysis, has been found to be 43% [30, 33].

Due to high CaO content, the SiO_4 tetrahedral network is completely broken ($Q^n = Q^0$ in SiQ^n) in the glass present in the ground-granulated blast furnace slag. The slag shows latent hydraulic activity, that is, it exhibits cementitious behaviour in the presence of water. In contrast, the network is mostly intact in the case of Class F fly ash (($Q^n = Q^3$ and Q^4, in SiQ^n) and it shows pozzolanic behaviour. It behaves like cement after a reaction with alkaline oxides; for example, with portlandite ($Ca(OH)_2$) formed during cement hydration reactions, alkali activator used in geopolymer synthesis, etc. [11, 46]. Usually, the amorphous substance in GGBFS and coal fly ash is the active part and determines the reactivity; a higher amount of glassy phase is associated with higher reactivity [11, 46, 47]. The presence of a small proportion of crystalline material finely dispersed in the glass is reported to improve grindability or reactivity or both [11]. Different methods are used to improve reactivity of fly ash and GGBFS and these include: mechanical/mechanochemical activation, microwave treatment, thermal

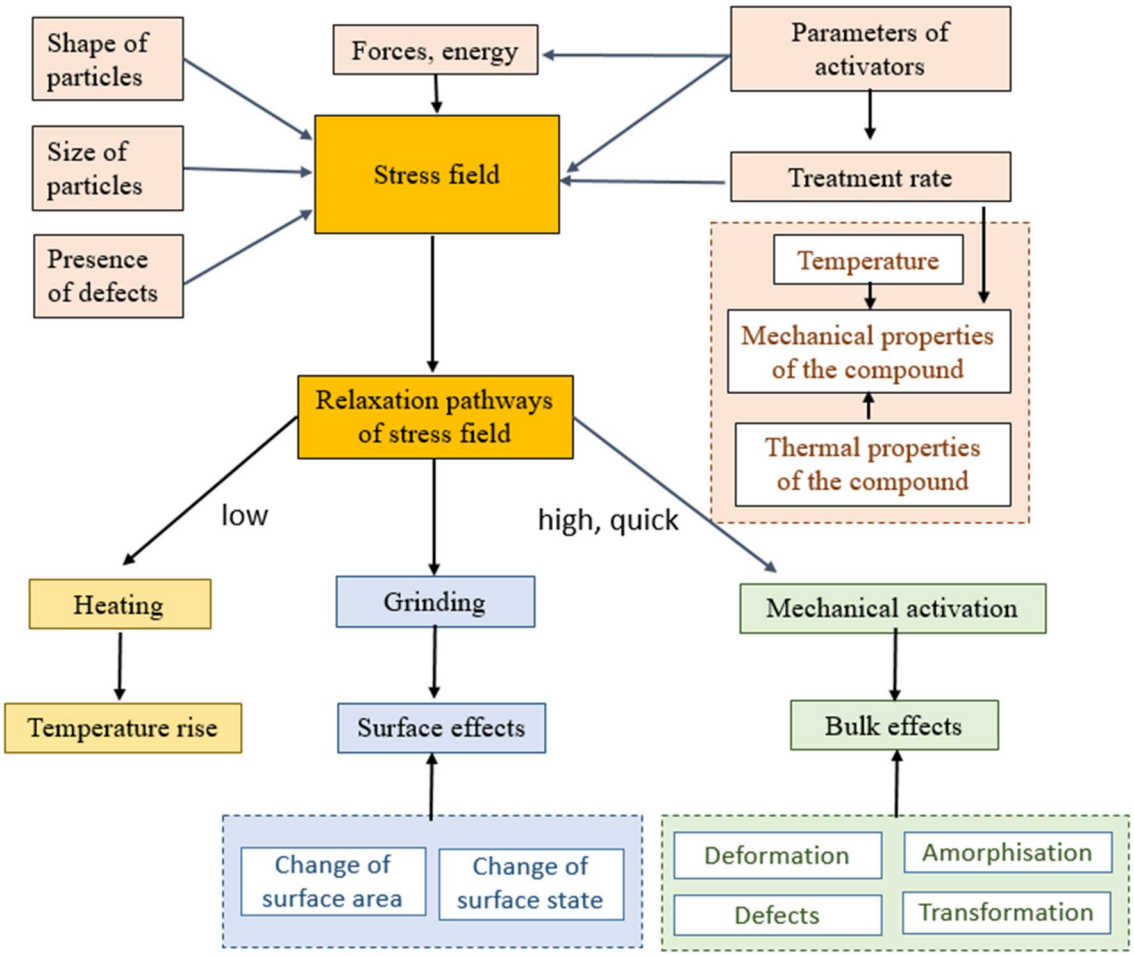

Fig. 2 Stress field created during milling and its relaxation pathways (heating, grinding, and mechanical activation) (adapted from ref. [4, 5])

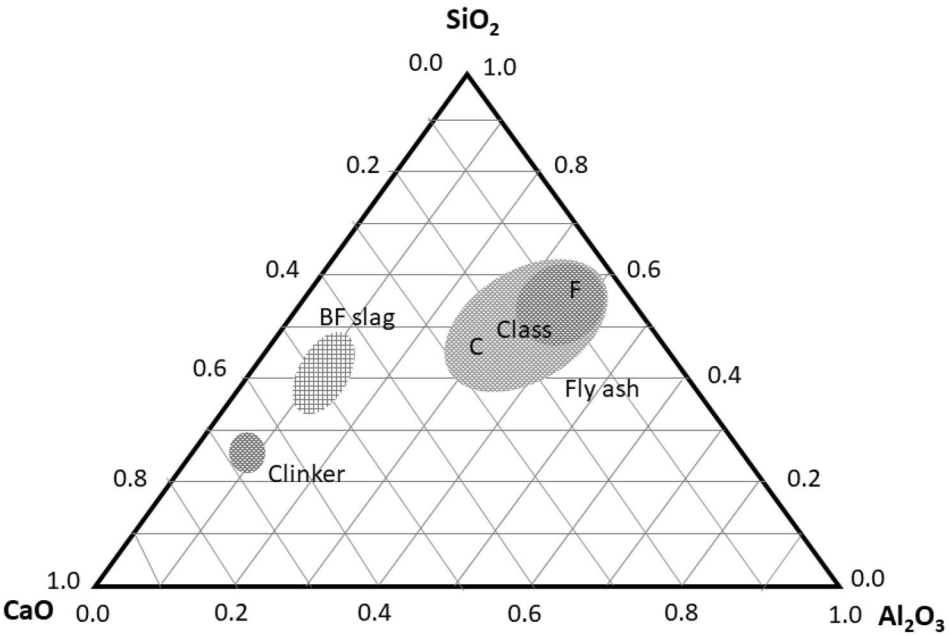

Fig. 3 Schematic representation of the chemical composition of blast furnace slag and Class F fly ash in the ternary SiO_2–Al_2O_3–CaO diagram. Typical composition regimes of Class C fly ash and cement clinker are also included for comparison (adapted from ref. [41])

activation, chemical activation, addition of a more reactive component and reaction (hydration/curing) temperature [46, 47]. Various methods of reactivity determination are reviewed [30, 46]. Isothermal conduction calorimetry which measures rate of heat evolved (dq/dt) as a function of reaction (slag hydration, fly ash geopolymerisation) time is widely used to assess alteration in reactivity due to mechanical activation [25, 27, 30, 31, 36, 37].

4 Peculiarities in Mechanical Activation

Peculiarities in the mechanical activation of ground-granulated blast furnace slag (GGBFS) and a Class F Indian fly ash (FA) are illustrated here using three examples: (a) hydration of attrition-milled and ball-milled GGBFS; (b) geopolymerisation of raw, classified, attrition-milled, and vibratory-milled fly ash; and (c) role of mechanical activation and temperature in geopolymerisation of fly ash. The first example is used to demonstrate the role of milling energy and the environment (presence of water) and how it influences the hydration of neat slag. The second example emphasises different mechanical processing treatments, the significance of the amorphous phase, and fly ash reactivity as manifested during the geopolymerisation reaction. Lastly, the relative importance of the different forms of energy, namely mechanical and thermal, is highlighted.

4.1 Attrition Milling vs. Ball Milling of Ground-Granulated Blast Furnace Slag

Stressing models characterised by the 'frequency' of stress events and the 'stress energy' acting at each event have been found useful to explain size reduction and mechanical activation behaviour in different mills with moving media [39, 48–52]. Attrition mill and ball mill (refers to a conventional ball mill all through) differ in terms of specific milling energy (E) which is the product of stress intensity (SI) and stress number (SN). SI is a measure of the kinetic energy of the media and SN indicates the probability of collision (frequency of stress events). Accordingly, E that determines energy transfer in the mill can be represented by the following simplified equations [50, 53].

$$E \propto \text{SI.SN} \tag{4}$$

$$E \propto \left(d_M^3 \rho_M v_t^2\right).\left(N\left(\frac{d_{50}}{d_M}\right)^2 t\right)^2 \tag{5}$$

(where d_M and ρ_M are the diameter and density of the media, d_{50} is the median size of feed, N is mill rpm, and v_t is peripheral speed). The proportionality constant in Eq. 5 depends on media filling volume (φ_m), media bed porosity (ε), volume concentration (c_v) of solid, etc. [50, 52].

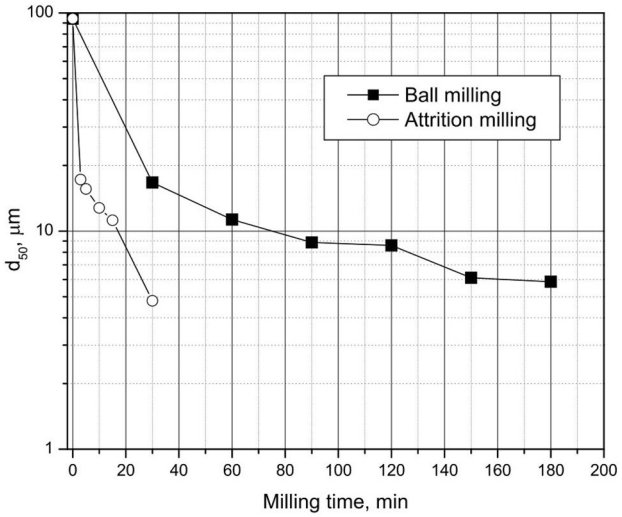

Fig. 4 Comparison of milling behaviour of slag during ball milling and attrition milling for the same initial feed size (Milling conditions: Ball milling—2000 g slag, 25–30 mm steel media, ball to powder ratio ~ 10, rpm 30–40 min^{-1}, dry mode; Attrition milling—150 g slag, 2 mm steel media, ball to powder ratio ~ 12, rpm 1000 min^{-1}, wet mode, solid to liquid ratio (v/v) ~ 0.25)

Under typical attrition milling (PE75, Netzsch GmbH; 2 mm steel media, disc type agitator, rpm 1000) and laboratory ball milling (AIM441, AIMIL India, 25–30 mm steel media, rpm 30–40) conditions, for the initial GGBFS feed size of 100 µm, the ratio $E_{Attritionmill}/E_{Ballmill}$ is $> 10^2$ (assuming proportionality constant in Eq. 5 to be the same for the two mills); means milling energy in the attrition mill is two orders of magnitude higher than ball mill. The d_{50} vs milling time results for the attrition and ball milling of GGBFS (Fig. 4) demonstrate the effect of milling energy (E) on size reduction kinetics. The kinetics is not only faster in the attrition mill but also a much lower size which does not appear feasible in the ball mill even after very prolonged milling can be achieved. Since attrition milling is carried out in wet conditions, the presence of water may further assist in size reduction [2, 10]. Further, it may be added that for a wide spectrum of milling conditions ($\varphi_m = 0.3 - 0.5$, $\varepsilon = 0.25 - 0.4$, and $c_v = 0.2 - 0.6$), the proportionality constant in Eq. 5 varies between ~ 0.3 and 2.5 (out of 60 tried combinations, about 50% of calculated values were in the range 1 ± 0.3). The ratio of maximum and minimum value of the proportionality constant, ~ 6 is much less than $E_{Attritionmill}/E_{Ballmill} > 10^2$. Therefore, attrition milling is expected to be more efficient and the comparison trend (Fig. 4) is expected to prevail.

The effect of milling devices goes much beyond size reduction [31]. This is revealed by the isothermal conduction

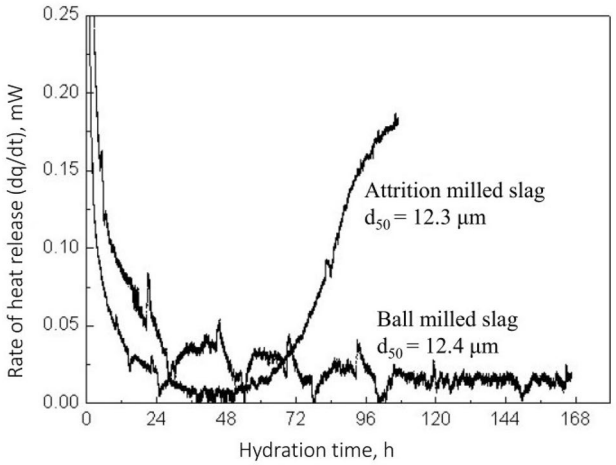

Fig. 5 Hydration of attrition-milled and ball-milled slag of similar median size (d_{50}) as revealed by isothermal conduction calorimetry [31]

calorimetric studies aimed to study hydration of milled slag in water under identical condition (7 g slag in 21 ml water, without any chemical additive). In spite of similar size distribution and d_{50} values (d_{50} ~ 12 µm), the attrition-milled slag shows distinctly different heat release responses vis-à-vis ball-milled slag (Fig. 5); the higher heat release for the attrition-milled slag indicates its higher reactivity. The slag hydration increases with an increase in attrition milling time and the 30 min slag hydrates completely after 28 days (Fig. 6). This was an accidental finding and quite contrary to the literature [11, 31, 54], where it has been reported that if GGBFS is placed in water alone, it dissolves to a small extent and a protective film is quickly formed which inhibits further hydration even for years. Complete hydration of attrition-milled GGBFS (reconfirmed recently [55, 56]) lead to the fundamental question, what is so different in attrition milling—milling energy, the presence of water, or both? Earlier, Song and Jennings [57] investigated the hydration of GGBFS in deionized water during wet ball milling for 28 days. Milling did improve the hydration but hydration stopped after 14 days and only a partial (~ 15%) hydration was obtained. In a more recent study, Singla et al. [58] reported that GGBFS of d_{50} ~ 5 µm (less than attrition-milled GGBFS, Fig. 5) obtained after dry vibratory milling (also a high-energy mill) did not hydrate in neat condition, thus signifying the role of water. It appears that the complete hydration of the attrition-milled GGBFS is favoured by the combined effect of milling energy and the presence of water.

The hydration product of attrition-milled slag has been found to be distinctly different from the ball-milled GGBFS

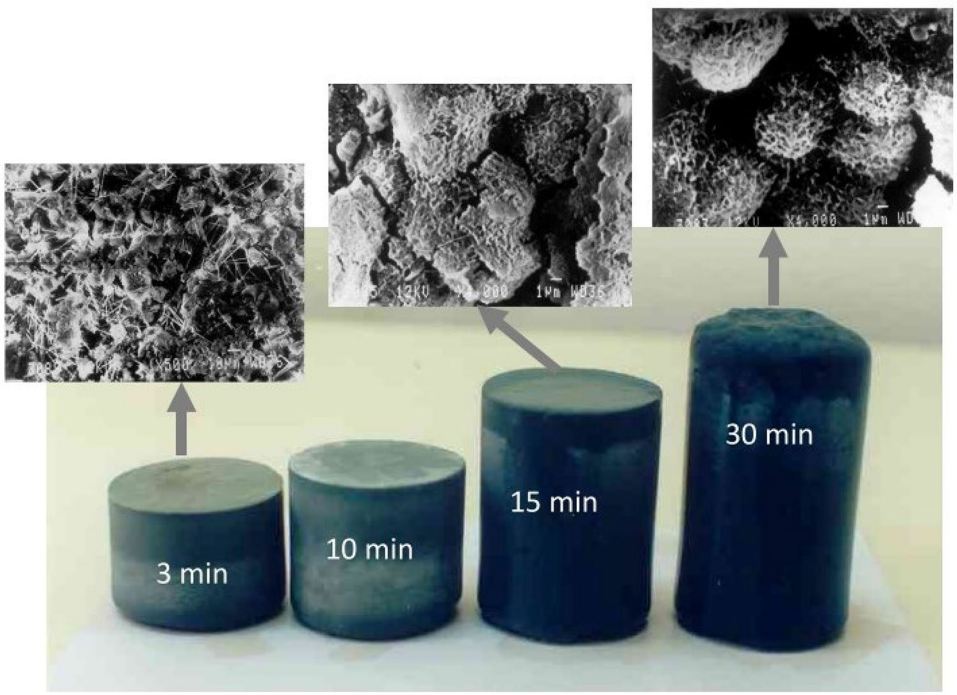

Fig. 6 Hydration products of mechanically activated blast furnace slag attrition milled for 3, 10, 15, and 30 min. Hydration was carried out for 28 days in polyvinyl chloride (PVC) bottles. The products correspond to same (100 g) of the milled slag. SEM micrographs (inserts) were recorded from broken pieces of the hydration products. Unreacted/partially reacted angular particles can be seen for the 3 min sample. Completely hydrated particles which appear as gel are visible for the 30 min sample

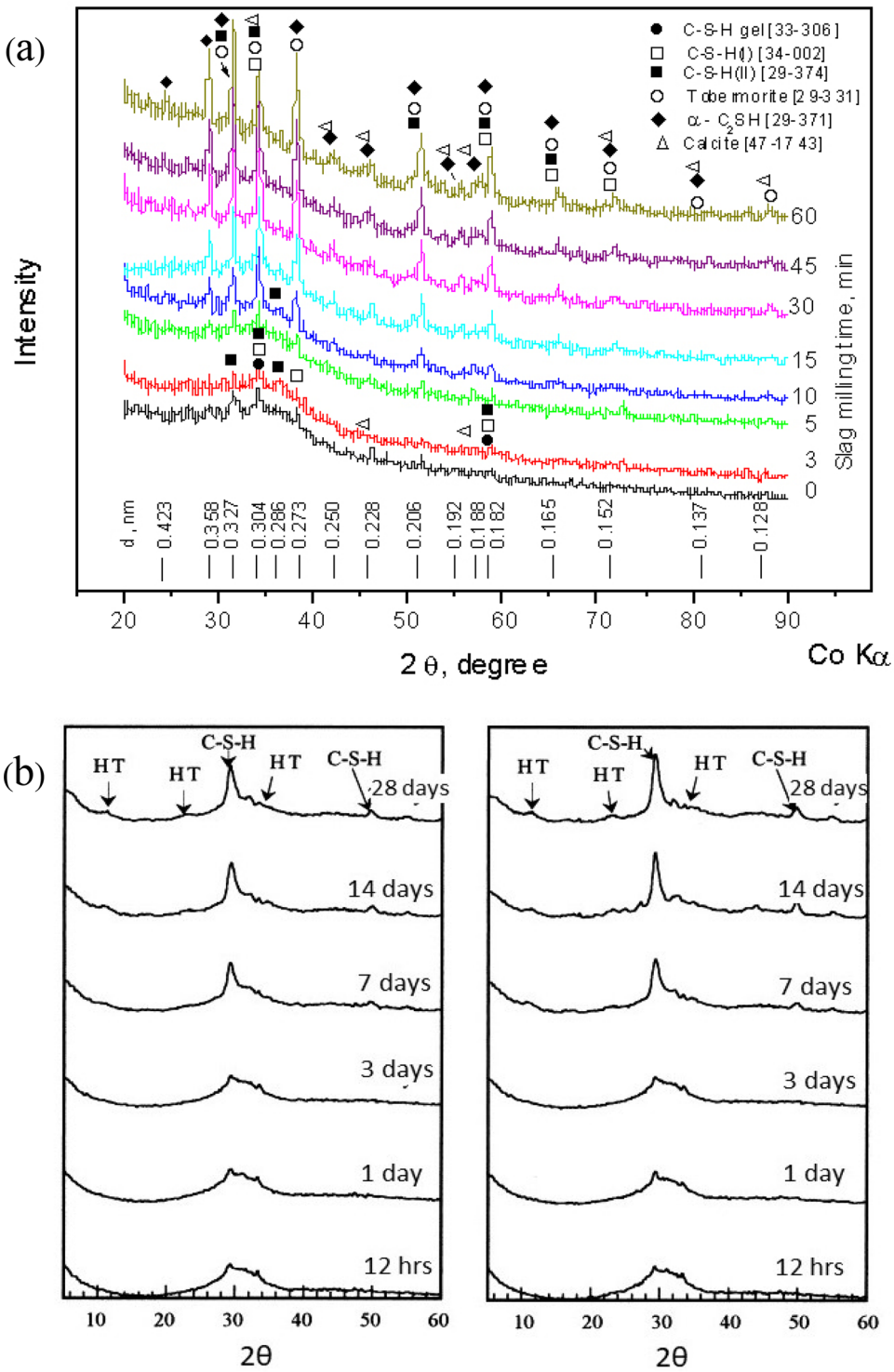

Fig. 7 Powder XRD diffraction patterns: **a** GGBFS attrition milled for different durations and after 28 days hydration [31], and **b** GGBFS rolled in a wet ball mill without (left) and with (right) steel media (adapted from ref. [50])

(Fig. 7a and b). It is more crystalline and its crystallinity increases with increased milling time [31, 57]. Interestingly, the hydration product of attrition-milled slag shows the presence of α-C_2SH which forms only under hydrothermal conditions [59]. The presence of hydrotalcite ($Mg_6Al_2(CO_3)(OH)_{16}{\cdot}4H_2O$) is reported in the hydration product of

ball-milled slag [57] and in the hydrated cement paste with vibratory-milled slag [58]. Conflicting reports are available on its occurrence in the hydration product of neat attrition-milled slag [31, 56]. Hydrotalcite is not present in freshly prepared cement paste and its presence is possibly related to the environment in which hydration is done (closed bottles [31] or normal ambient atmosphere [56]) and ageing time [60]. When ageing is done in open atmosphere, occurrence of calcite and aragonite are also observed indicating severe carbonation [56]. It is not clear if milling energy has a role to play as milling is carried out under milder condition (zirconia ball, density ~ 5.6 g/cm^3, size -10 mm, 8 mm, 5 mm and 3 mm media in the ratio = 1:3:6:2, 400 rpm) [56] compared to other study (steel ball, density—7.8 g/cm^3, size—2 mm, rpm—100) [31] (see Eqs. 4 and 5 for the significance of these variables in the context of milling energy).

The structural changes induced in GGBFS during attrition milling are not well understood to date. Since the slag is mostly glassy in character, X-ray powder diffraction does not provide an answer [31]. The zeta potential of the slag is altered during milling and points towards surface activation [31]. Preliminary experiments by the author indicates enhanced dissolution of slag after attrition milling. In the literature, it has been reported that the slags with nano-dispersion of crystalline phases show higher reactivity [11]. In metallic glasses, stress-induced localised perturbations in the structure are observed [61–63]. No such study is available on GGBFS and is required to find an answer.

4.2 The Distinction Between the Effect of Size and Mechanical Activation

Geopolymers, aluminosilicate polymers with general formula $M_n[-(Si-O_2)_z-Al-O]_n.wH_2O$ (where M is an alkaline element, z is 1, 2, or 3, and n is the degree of polymerisation), have steadily developed as a new class of green building material due to their versatile properties and low environmental impact [14, 30]. The utilisation of fly ash as an alternative aluminosilicate raw material is of interest to the development of greener geopolymers. Various methods of fly ash activation (mechanical, chemical, thermal, etc.) are available to tailor geopolymer properties [30, 46, 64] (also S27-S60]. The focus here is on mechanical processing which include high speed air classification (CFA) and mechanical activation using attrition milling (AMFA) and

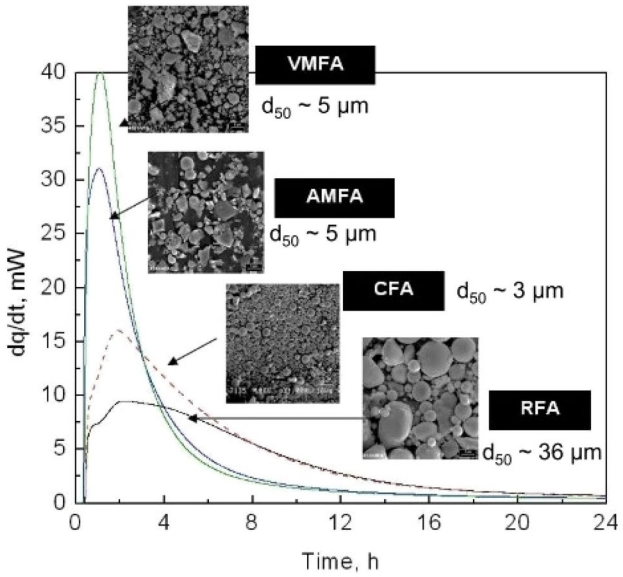

Fig. 8 Calorimetric response in terms of rate of heat evolved (dq/dt) with geopolymerisation time for raw fly ash (RFA), air-classified (3000 rpm) fly ash (CFA), attrition-milled fly ash (AMFA), and vibratory-milled fly ash (VMFA) (the insert shows morphology (SEM micrographs) and median size (d_{50}) (adapted from ref. [35])

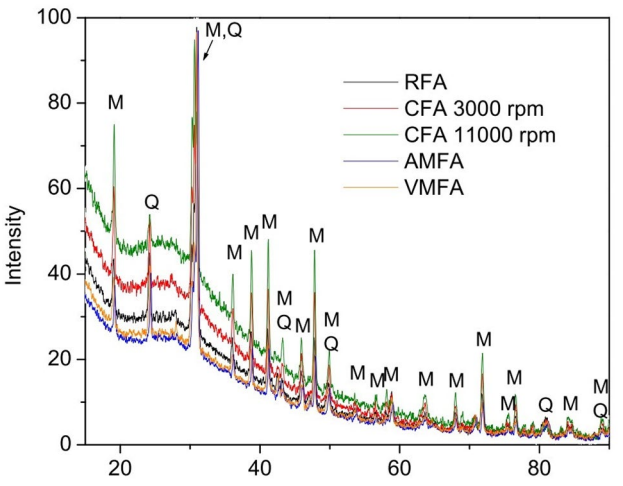

Fig. 9 Powder X-ray diffraction (XRD) patterns of raw fly ash (RFA), air-classified fly ash (CFA), attrition-milled fly ash (AMFA), and vibratory-milled fly ash (VMFA) used for isothermal calorimetry (Fig. 8) (Q—α-quartz (SiO_2), M—mullite ($3Al_2O_32SiO_2$ or $2Al_2O_3$ SiO_2) [35]

eccentric vibratory milling (VMFA) [23, 35, 37]. Classification separates fly ash particles which cool faster during coal combustion and have higher glass phase content. The raw fly ash used to generate mechanically processed samples is used as a reference. The median size (d_{50}) of RFA, CFA, AMFA, and VMFA was 35, 2.8, 4.3, and 5 µm, respectively.

To illustrate the effect of mechanical processing, Fig. 8 shows the calorimetric response (rate of heat evolved vs. geopolymerisation time) of the fly ash samples during geopolymerisation at 60 °C. In terms of fly ash reactivity (maximum rate of heat evolution, $(dq/dt)_{max}$) and median size, the fly ash samples can be arranged as VMFA (5) > AMFA (4.3) > CFA (2.8) > RFA (36) (the number in parentheses indicate particle size). This reactivity sequence is preserved in geopolymers prepared with mixture of RFA and mechanically processed fly ash [35]. The reactivity, CFA > RFA, is quite understandable and may be attributed to the smaller particle size and higher glass content of CFA. In spite of the higher particle size, the higher reactivity of AMFA and VMFA over CFA is intriguing. Based on characterisation by XRD, FTIR, and XPS, a possible explanation has been presented in terms of the alternation in the nature of the glass phase [27, 35, 37, 65–67]. In the XRD patterns (Fig. 9) [35], the change is manifested by a reduction in the background attributed to the glass phase in AMFA and VMFA vis-à-vis RFA (as expected, the background increases in CFA due to its higher glass content). To this date, the origin of higher reactivity VMFA vis-à-vis AMFA which is manifested in the development of very high-strength geopolymers remains elusive and calls for more systematic in-depth characterisation studies. Possibly, there are lessons to be learned from the studies on metallic glasses where stress-induced crystallisation and segregation are reported [61, 63, 68]. Stress and thermally activated crystallisation of mullite is indicated [27, 35, 65]. Additionally, it may be noted that finely dispersed mullite and quartz (produced by milling or through localised crystallisation) may act as nucleation site for geopolymer gel and favour its formation [30].

4.3 Role of Mechanical Activation vis-à-vis Temperature in Geopolymerisation of Fly Ash

In recent times, there have been attempts to combine mechanical activation with temperature and it is observed that reaction path and activation energy can be altered in solid–solid mechanochemical reactions [69–71] and for the reactions involving the activated solids [72–75]. In general, individually, both mechanical activation and reaction temperature enhances the rate of reactions. However, their relative efficacy is open to debate when used simultaneously. For example, during the hydrothermal leaching of wolframite, the efficacy of mechanical activation increases with the leaching temperature [76]. In contrast, for bauxite and aluminium hydroxide leaching in alkali, mechanical activation is found to be more effective at a lower temperature [74, 77].

The beneficial effect of an increase in curing temperature (27 to 60 °C) on the compressive strength of vibratory-milled fly ash-based geopolymer is reported [37]. The combined effects of mechanical activation and temperature on the dissolution process of a Class F fly ash were investigated by Cristelo et al. [65]. Increasing dissolution temperature proved to be very effective in terms of bulk mass dissolved, with higher dissolution values after 16 h, at 80 °C, than after 90 days, at 20 °C. This indicates that the increased cost of higher curing temperatures is mitigated by the significantly shorter curing periods [65]. Relative efficacy of mechanical activation vis-à-vis geopolymerisation temperature was investigated by Kumar et al. [30] using reactivity maps and the highlights of the analysis and significance are presented here.

For the purpose of analysis, geopolymerisation of Class F fly ash samples obtained after vibratory milling for seven different durations (t_{MA} = 0, 5, 15, 30, 60, 90, 120 min) was investigated at seven reaction temperatures (T_{GP} = 27, 32, 37, 42, 47, 53, 60 °C) using isothermal conduction calorimetry. The response was monitored for 24 h and reactivity map, tagged in terms of t_{MA} and T_{GP}, was created for the reaction heat evolved (Q) or fraction of fly ash reacted (α) with geopolymerisation time (t) (Fig. 10). At any specific geopolymerisation time, the value of fraction reacted (α) increases with both t_{MA} and T_{GP}. The same value of α can be obtained for different combinations of t_{MA} and T_{GP} as evident from the iso-conversion map (Fig. 11) in which the time required (t_α) for the maximum achievable values α without activation is plotted (i.e. for α = 0.076, 0.093, 0.207, 0.334, 0.505, 0.640, and 0.795). The iso-conversion map in Fig. 11 is quite revealing as it gives an idea of the time required to achieve the same values of α under different combinations of t_{MA} and T_{GP}.

In order to assess the relative importance of t_{MA} and T_{GP}, a detailed analysis was undertaken. The efficacy was assessed using the following empirical parameters (η and R) defined for fraction reacted (α) at t = 24 h for each of (t_{MA},T_{GP}) conditions:

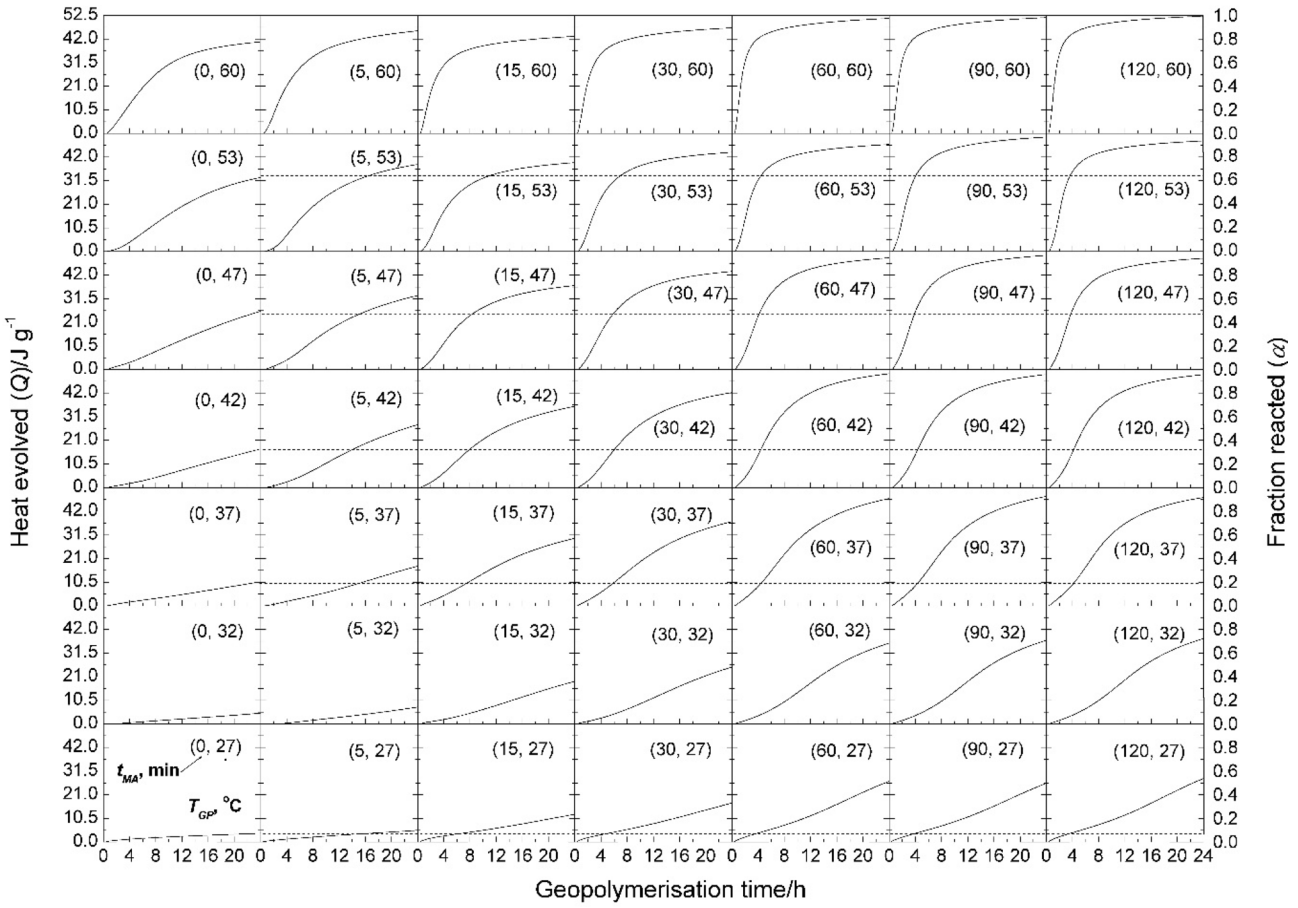

Fig. 10 Map showing heat evolved (Q) and fraction reacted (α) with geopolymerisation time for different mechanical activation time (t_{MA}) and geopolymerisation temperature (T_{GP}). The plots are tagged as (t_{MA},T_{GP}) [30]

$$\eta = \left(\alpha_{(t_{MA},T_{GP})} - \alpha_{(0,T_{GP})}\right)\left(\frac{1440}{t_{MA}}\right) \tag{6}$$

$$R = \left(\frac{\alpha_{(t_{MA},T_{GP})} - \alpha_{(0,T_{GP})}}{\alpha_{(t_{MA},T_{GP})} - \alpha_{(t_{MA},27)}}\right) \tag{7}$$

η indicates a normalised change in fraction reacted (after $t = 24$ h) due to mechanical activation at a specific geopolymerisation temperature. The normalisation is done with respect to mechanical activation time (t_{MA}), and the factor 1440 (the minute equivalent of 24 h) is introduced to make the parameter dimensionless. Interestingly, the variation of η with T_{GP} shows a maximum between 37 and 42 °C; with increasing t_{MA}, the maximum shifts towards lower value (Fig. 12). Further, the sensitivity of η on T_{GP} decreases with an increase in t_{MA}.

The parameter R signifies the relative importance of t_{MA} vis-a`-vis T_{GP} (taking 27 °C as a reference). The variation of R with T_{GP} (Fig. 13) can be used to delineate the regime of the dominance of t_{MA} ($R > 1$) and T_{GP} $R < 1$ (Figs. 13 and 14). It is evident from the figures that mostly $R > 1$ values are observed below 47 °C for a milling time 15 min or more. The highest value of R (3.0–3.5) is achieved at 32 °C. The highest values of R do not yield the highest values of α and a judicious selection of mechanical activation time and geopolymerisation temperature is required to achieve desired value of α. If geopolymer structure and properties values are superimposed on the maps (Figs. 10 and 14) it

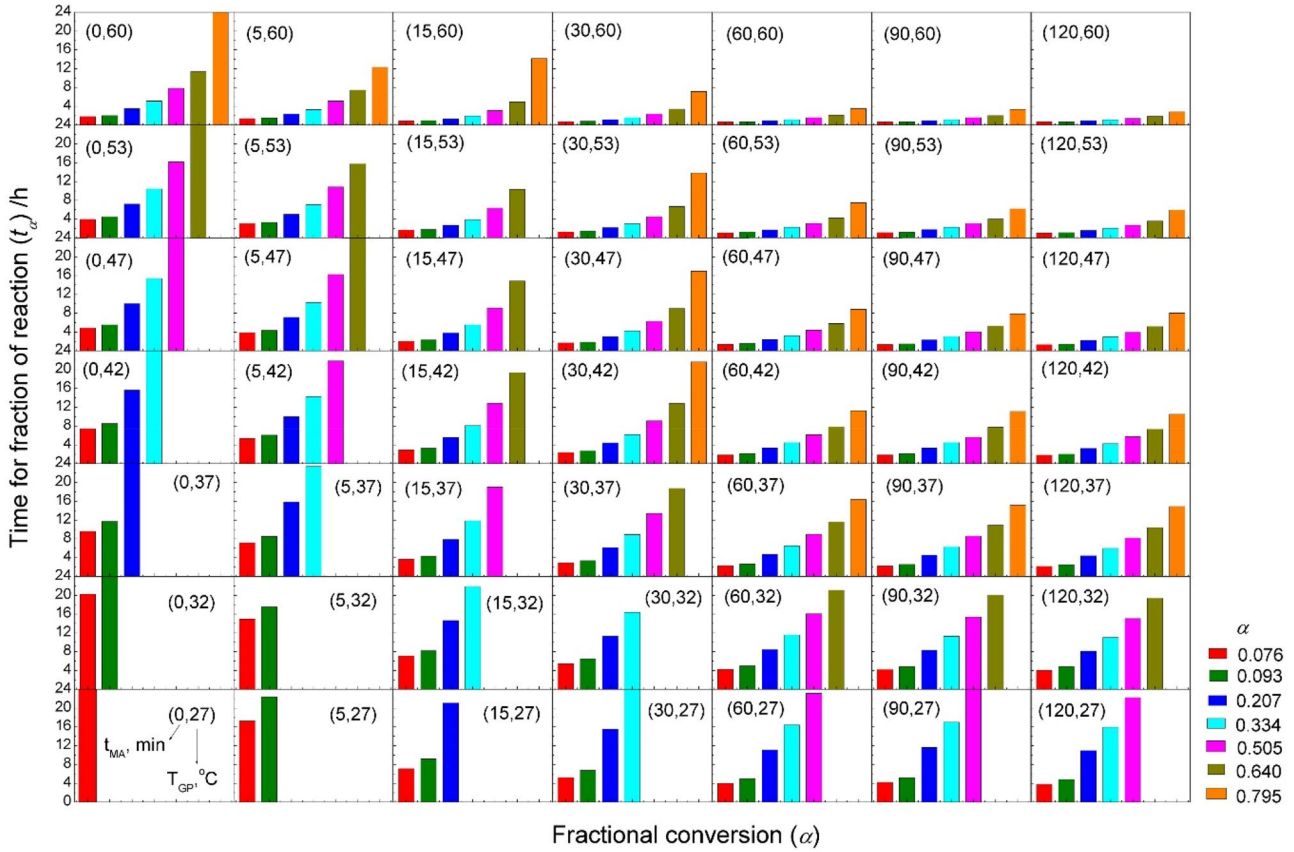

Fig. 11 Iso-conversion map showing the time required to achieve different values of fractional conversion after 24 h ($\alpha_{t=24h}$) under different mechanical activation times (t_{MA}) and geopolymerisation temperatures (T_{GP}). The plots are tagged as (t_{MA},T_{GP}) [30]

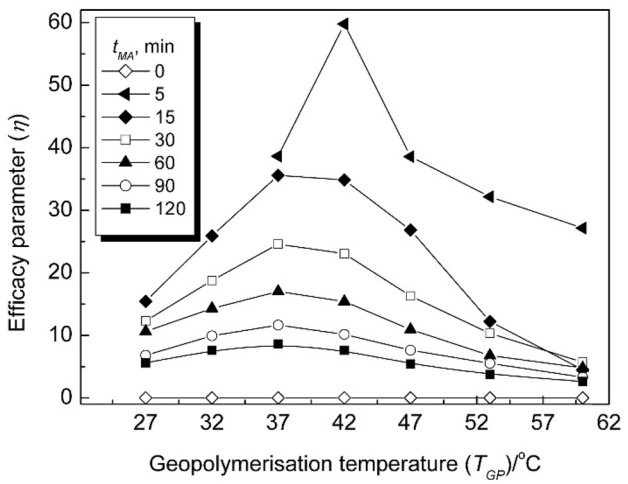

Fig. 12 Variation of efficacy parameters η with milling time (t_{MA}) and geopolymerisation temperature (T_{GP}) [30]

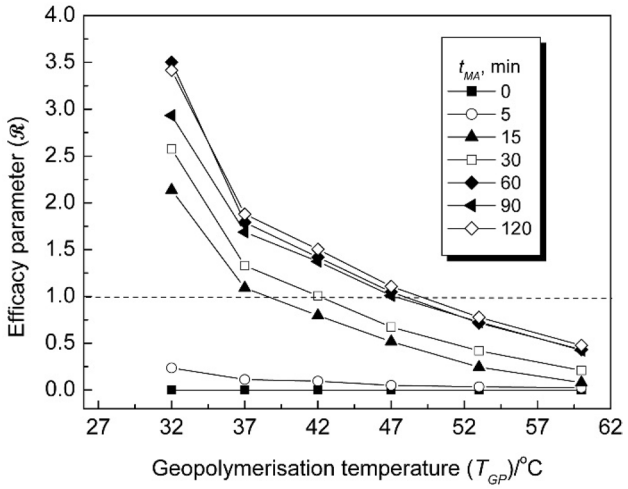

Fig. 13 Variation of efficacy parameters R with milling time (t_{MA}) and geopolymerisation temperature (T_{GP}) [30]

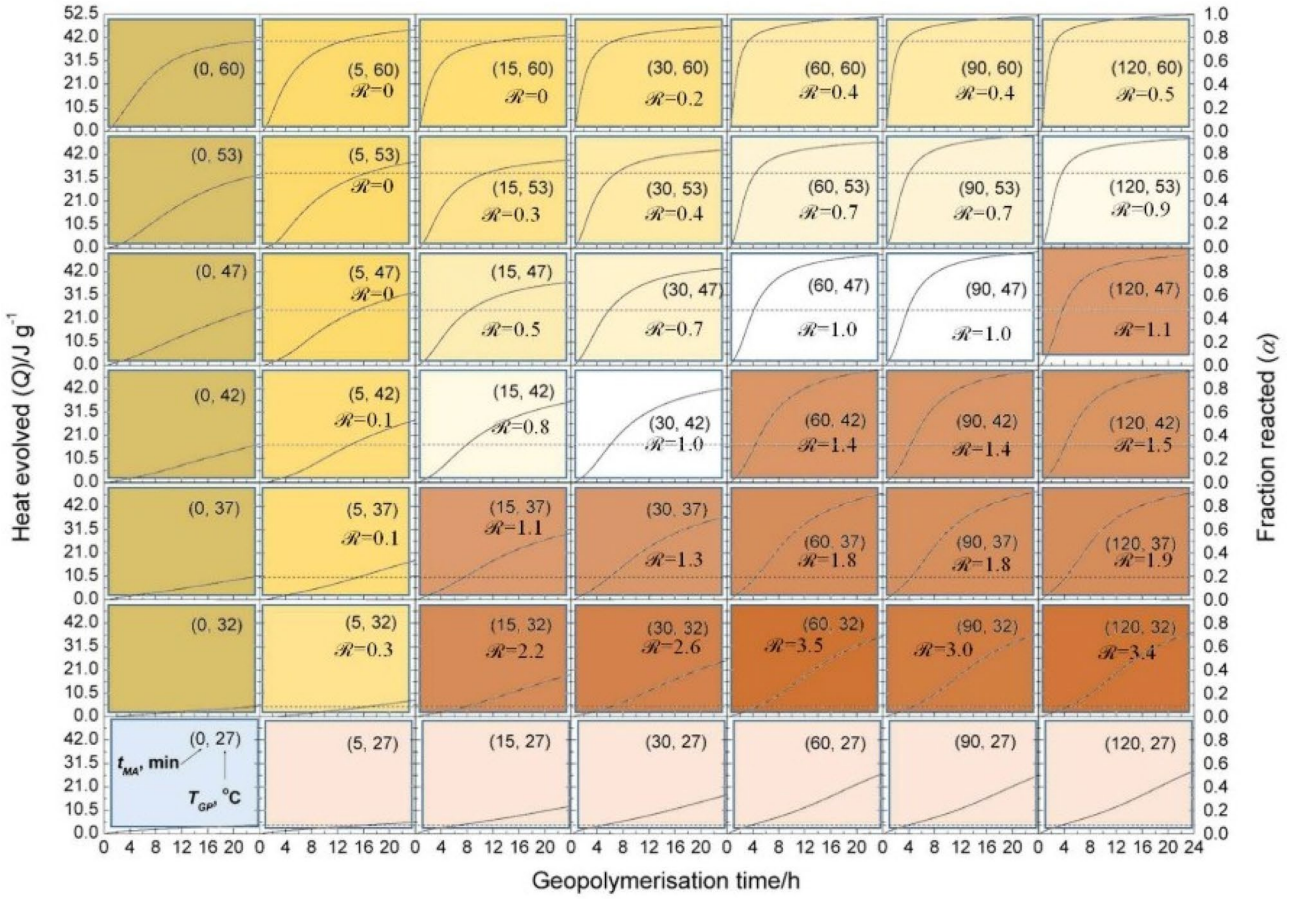

Fig. 14 Superimposition of relative efficacy parameter R on the heat evolved (Q) and fraction reacted (α) map for different mechanical activation times (t_{MA}) and geopolymerisation temperatures (T_{GP}). Different shades of yellow, white, and brown are used to delineate regions with $R =< 1, \sim 1$, and > 1, respectively

can help towards tailoring the geopolymer properties based on calorimetric data.

5 Concluding Remarks

Illustrative examples from mechanical activation of GGBFS and FA are presented to elucidate the role of the milling device, energy, and mill environment. Even though the beneficial effect of mechanical activation on the properties of blended cement and geopolymers is well known, the understanding of linkages in the tetrahedron, milling—structural changes—reactivity—product properties is generally lacking. The pointers on mechanically induced physicochemical changes in the predominantly amorphous phases require further probing. Characterisation techniques (XRD and FTIR) are inadequate and needs to be clubbed with other microscopic (TEM, AFM) and spectroscopic studies which can probe the local structure at nano and atomic scale. In this context, research on deformation in metallic glasses is noteworthy and needs consideration. The findings reported in this paper on coupling mechanical activation with reaction temperature are preliminary and in-line with the current trends whereby mechanical activation is used together with other forms of energies (light, acoustic, etc.). The concept of calorimetric maps developed for geopolymerisation may have general applicability in materials synthesis, especially if the maps can be superimposed with structure and properties.

Acknowledgements The author is grateful to the entire team of NMITLI project at CSIR-National Metallurgical Laboratory, Jamshedpur (India), notably Dr. Sanjay Kumar (presently Head, MER Division), Dr. T.C. Alex (Mechanochemistry Group), Dr. B. Ravi Kumar, Dr. Swapan Das, Dr. T. Mishra (Characterisation team), and I.B. Mishra (Civil Engineering). Guidance and support from Professor S.P. Mehrotra (formerly Director, CSIR-NML) is gratefully acknowledged. Late Prof. Ramachandra Rao and Prof. P.C. Kapur mentored the project. The author would like to acknowledge support from Professor Rajiv Shekhar (former Director, IIT-ISM, Dhanbad).

Declarations

Conflict of interest There is no conflict of interest.

References

1. Momber A W, *J Mater Sci* **45** (2010) 750. https://doi.org/10.1007/s10853-009-3996-4
2. Baláž P, Achimovičová M, Baláž M, Billik P, Cherkezova-Zheleva Z, Criado J M, Delogu F, Dutková E, Gaffet E, Gotor F J, and Kumar R, *Chem Soc Rev* **42** (2013) 7571. https://doi.org/10.1039/c3cs35468g
3. Baláž P, *Mechanochemistry in nanoscience and minerals engineering*, Springer-Verlag, Berlin Heidelberg (2008).
4. Boldyreva E, *Faraday Discuss* **241** (2022) 9. https://doi.org/10.1039/d2fd00149g
5. Michalchuk A A, Boldyreva E V, Belenguer A M, Emmerling F, and Boldyrev V V, *Front Chem* **9** (2021) 359. https://doi.org/10.3389/FCHEM.2021.685789/BIBTEX
6. Senna M, *ChemTexts* **3** (2017) 1. https://doi.org/10.1007/s40828-017-0041-0
7. Pagola S, *Crystals* **13** (2023) 124. https://doi.org/10.3390/CRYST13010124
8. Singla R, Alex T C, and Kumar R, *Powder Technol* **360** (2020) 337. https://doi.org/10.1016/J.POWTEC.2019.10.035
9. Baláž M (2021) Environmental Mechanochemistry, 1st ed. Environ Mechanochemistry. doi: https://doi.org/10.1007/978-3-030-75224-8
10. Juhász AZ, Opoczky L (1990) Mechanical Activation of Minerals by Grinding, Pulverizing and Morphology of Particles. Ellis Horwood Limited
11. Taylor H F W, *Cement chemistry*, Thomas Telford Publishing, London (1997).
12. Sekulić Ž, Popov S, Uričić M, and Rosić A, *Mater Lett* **39** (1999) 115. https://doi.org/10.1016/S0167-577X(98)00226-2
13. Matthes W, Vollpracht A, Villagrán Y, Kamali-Bernard S, Hooton D, Gruyaert E, Soutsos M, and De Belie N, *RILEM State Art Rep* **25** (2018) 1. https://doi.org/10.1007/978-3-319-70606-1_1/COVER
14. Scrivener K L, John V M, and Gartner E M, *Cem Concr Res* **114** (2018) 2. https://doi.org/10.1016/J.CEMCONRES.2018.03.015
15. Opoczky L O, Verdes S, and Török K M, *Powder Technol* **48** (1986) 91. https://doi.org/10.1016/0032-5910(86)80069-9
16. Malhotra V M, and Hammings R T, *Cem Concr Compos* **17** (1995) 23. https://doi.org/10.1016/0958-9465(95)95757-Q
17. Helmuth R A, Whiting D A, Dubovoy V S, Tang F J, and Love H, *ASTM Spec Tech Publ* (1986). https://doi.org/10.1520/STP36394S
18. Giergiczny Z, Werynska A (1989) Influence of fineness of fly ashes on their hydraulic activity. ACI Spec Publ SP-114. https://doi.org/10.14359/1869
19. Energetically modified cement. In: Wikipedia. https://en.wikipedia.org/wiki/Energetically_modified_cement. Accessed 24 Jan 2023
20. Sobolev K, *Mater Technol Adv Perform Mater* **14** (1999) 191. https://doi.org/10.1080/10667857.1999.11752838
21. Atiş C D, Görür E B, Karahan O K, Bilim C, İlkentapar S E, and Luga E, *Constr Build Mater* **96** (2015) 673. https://doi.org/10.1016/J.CONBUILDMAT.2015.08.089
22. Kumar R, Kumar S, and Mehrotra S P, Mechanical activation in blended cement processing. in *Front*, (eds) Kumar R, Srikanth S, and Mehrotra S P, Mechanochemistry Mech Alloy, CSIR-National Metallurgical Laboratory, Jamshedpur, India, Jamshedpur (2011), p 294.
23. Kumar R, Kumar S, Alex T C, Srikanth S, and Mehrotra S P, Process innovations using mechanical activation of minerals and wastes. in *Exp Theor Approaches to Mod*, (eds) Mulas G, and Delogu F, Mechanochemistry, Transworld Research Network, Chennai (2010), p 255.
24. Kumar S, Kumar R (2010) Tailoring geopolymer properties through mechanical activation of fly ash. In: Zachar J, Claisse P, Naik TR, Ganjian E (eds) Second Int Conf Sustain Constr Mater Technol. June 28 - June 30, 2010, Univ. Politec. delle Marche, Ancona, Italy. Coventry University and The University of Wisconsin Milwaukee Centre for By-products Utilization, p 607
25. Kumar S, Kumar R, Bandopadhyay A, Alex T C, Kumar B R, Das S K, and Mehrotra S P, *Cem Concr Compos* **30** (2008) 679. https://doi.org/10.1016/J.CEMCONCOMP.2008.05.005
26. Kumar S, Kumar R, and Bandopadhyay A, *Resour Conserv Recycl* **48** (2006) 301. https://doi.org/10.1016/J.RESCONREC.2006.03.003
27. Kumar S, Mucsi G, Kristály F, and Pekker P, *Adv Powder Technol* **28** (2017) 805. https://doi.org/10.1016/J.APT.2016.11.027
28. Kumar S, García-Triñanes P, Teixeira-Pinto A, and Bao M, *Cem Concr Compos* **40** (2013) 7. https://doi.org/10.1016/J.CEMCONCOMP.2013.03.026
29. Mucsi G, Kumar S, Csőke B, Kumar R, Molnár Z, Rácz Á, Mádai F, and Debreczeni Á, *Int J Miner Process* **143** (2015) 50. https://doi.org/10.1016/J.MINPRO.2015.08.010
30. Kumar R, Kumar S, Alex T C, and Singla R, *J Therm Anal Calorim* **136** (2019) 1117. https://doi.org/10.1007/S10973-018-7736-3/FIGURES/9
31. Kumar R, Kumar S, Badjena S, and Mehrotra S P, *Metall Mater Trans B Process Metall Mater Process Sci* **36** (2005) 873. https://doi.org/10.1007/s11663-005-0089-x
32. Kumar R, Kumar S, Das A, Mishra T K, Cholavandan V, and Mehrotra S P, *Studies on reactivity of classified and mechanically activated fly ash (Project OLP- 064)*, Jamshedpur, India (2007).
33. Kumar R, Kumar S, and Mehrotra S P, *Resour Conserv Recycl* **52** (2007) 157. https://doi.org/10.1016/j.resconrec.2007.06.007
34. Kumar S, Bandopadhyay A, Rajinikanth V, Alex T C, and Kumar R, *J Mater Sci* **39** (2004) 3449. https://doi.org/10.1023/B:JMSC.0000026948.85440.cc
35. Kumar S, Kumar R, and Mehrotra S P, Geopolymers, fly ash reactivity and mechanical activation. in *Front Mechanochemistry Mech Alloy*, (eds) Kymar R, Srikanth S, and Mehrotra S P, CSIR-National Metallurgical Laboratory, Jamshedpur, India, Jamshedpur (2011), p 320.
36. Kumar S, Kumar R, Alex T C, Bandopadhyay A, and Mehrotra S P, *Adv Appl Ceram* **106** (2007) 120. https://doi.org/10.1179/174367607X159293
37. Kumar S, and Kumar R, *Ceram Int* **37** (2011) 533. https://doi.org/10.1016/j.ceramint.2010.09.038
38. Boldyrev V V, Polov S V, and Goldberg E L, *Int J Min Process* **44–45** (1996) 181.
39. Alex T C, Kumar R, Roy S K, and Mehrotra S P, *Adv Powder Technol* **19** (2008) 483. https://doi.org/10.1016/s0921-8831(08)60914-0
40. Alex T C, Kumar R, Roy S K, and Mehrotra S P, *Miner Process Extr Metall Rev* **37** (2016) 1. https://doi.org/10.1080/08827508.2015.1055626
41. Frances C, Le Bolay N, Belaroui K, and Pons M N, *Int J Miner Process* **61** (2001) 41. https://doi.org/10.1016/S0301-7516(00)00025-9
42. Guzzo P L, Ţălu Ş, Kulesza S, and Bramowicz M, *Jom* **75** (2023) 1333. https://doi.org/10.1007/s11837-022-05687-1

43. Tromans D, and Meech J A, *Miner Eng* **15** (2002) 263. https://doi.org/10.1016/S0892-6875(02)00017-1
44. Wang A, Zheng Y, Zhang Z, Liu K, Li Y, Shi L, and Sun D, *Engineering* **6** (2020) 695. https://doi.org/10.1016/j.eng.2019.08.019
45. Suraneni P, Burris L, Shearer C R, and Hooton R D, *ACI Mater J* **118** (2021) 157. https://doi.org/10.14359/51725994
46. Li Z, Xu G, and Shi X, *Fuel* **301** (2021) 121031. https://doi.org/10.1016/j.fuel.2021.121031
47. Giergiczny Z, *Cem Concr Res* **124** (2019) 10526. https://doi.org/10.1016/j.cemconres.2019.105826
48. Alex TC, Kumar R, Roy SK, Mehrotra SP (2012) Mechanical activation of Al-oxyhydroxide minerals - Physicochemical changes, reactivity and relevance to bayer process. In: Suarez CE (ed) Light Met. 2012. pp 15–19
49. Hoffmann U, Horst C, and Kunz U, Reactive Comminution. in *Integr*, (eds) Sundmacher K, Kienle A, and Seidel-Morgenstern A, Chem. Process-Synth Oper Anal Control, Wiley-VCH Verlag GmbH & Co KGaA (2005), pp 407–436.
50. Kwade A, *Powder Technol* **105** (1999) 14. https://doi.org/10.1016/S0032-5910(99)00113-8
51. Kwade A, *Chem Eng Technol* **26** (2003) 199. https://doi.org/10.1002/ceat.200390029
52. Kwade A, and Schwedes J, *Powder Technol* **122** (2002) 109. https://doi.org/10.1016/S0032-5910(01)00406-5
53. Mucsi G, *Chem Eng Res Des* **148** (2019) 460. https://doi.org/10.1016/J.CHERD.2019.06.029
54. Mehta P K, *Spec Publ* **114** (1989) 1. https://doi.org/10.14359/1835
55. Peuker U A, *Mater Sci Forum* **959** (2019) 177. https://doi.org/10.4028/WWW.SCIENTIFIC.NET/MSF.959.177
56. Wang Y, He X, Su Y, Tan H, Yang J, Lan M, Ma M, and Strnadel B, *Constr Build Mater* **167** (2018) 96. https://doi.org/10.1016/J.CONBUILDMAT.2018.01.178
57. Song S, and Jennings H M, *Cem Concr Res* **29** (1999) 159. https://doi.org/10.1016/S0008-8846(98)00212-9
58. Singla R, Kumar S, and Alex T C, *Waste Biomass Valorizat* **11** (2020) 2983. https://doi.org/10.1007/s12649-019-00580-6
59. Garbev K, Leon B, Beuchle G, and Peter S, *Wasser- und Geotechnol Nachrichten aus dem Inst für Tech Chemie* **1** (2002) 19.
60. Black L, Garbev K, and Gee I, *Cem Concr Res* **38** (2008) 745. https://doi.org/10.1016/J.CEMCONRES.2008.02.003
61. Stachurski H Z, *Fundamentals of amorphous solids-structure and properties*, Wiley-VCH Verlag GmbH & Co., Weinheim (2015).
62. Louzguine-Luzgin D V, Trifonov A S, Ivanov Y P, Lu A K, Lubenchenko A V, and Greer A L, *Sci Rep* **111** (2021) 1. https://doi.org/10.1038/s41598-021-92907-4
63. Jang D, and Greer J R, *Nat Mater* **93** (2010) 215. https://doi.org/10.1038/nmat2622
64. Grabias-Blicharz E, and Franus W, *Sci Total Environ* (2022). https://doi.org/10.1016/j.scitotenv.2022.160529
65. Cristelo N, Tavares P, Lucas E, Miranda T, and Oliveira D, *Compos Part B Eng* **103** (2016) 1. https://doi.org/10.1016/J.COMPOSITESB.2016.08.001
66. Temuujin J, Williams R P, and van Riessen A, *J Mater Process Technol* **209** (2009) 5276. https://doi.org/10.1016/j.jmatprotec.2009.03.016
67. Kanuchova M, Drabova M, Sisol M, Mosej J, Kozakova L, and Skvarla J, *Environ Prog Sustain Energy* **35** (2016) 1338. https://doi.org/10.1002/EP.12353
68. Linberg K, Röder B, Al-Sabbagh D, Emmerling F, and Michalchuk A A, *Faraday Discuss* **241** (2023) 178. https://doi.org/10.1039/D2FD00115B
69. Andersen J M, and Mack J, *Chem Sci* **8** (2017) 5447. https://doi.org/10.1039/c7sc00538e
70. Brügner O, and Walter M, *Phys Rev Mater* **2** (2018) 1. https://doi.org/10.1103/PhysRevMaterials.2.113603
71. Liu X, Shao Y, Zhang Y, Meng G, Zhang T, and Wang F, *Corros Sci* **90** (2015) 463. https://doi.org/10.1016/j.corsci.2014.04.016
72. Alex T C, Sasi Kumar C, Kailath A J, Kumar R, Roy S K, and Mehrotra S P, *Metall Mater Trans B* **42** (2011) 592. https://doi.org/10.1007/s11663-011-9494-5
73. Alex T C, Kumar R, Roy S K, and Mehrotra S P, *Hydrometallurgy* **144–145** (2014) 99. https://doi.org/10.1016/J.HYDROMET.2014.01.017
74. Kumar R, and Alex T C, *Metall Mater Trans B* **46** (2015) 1684. https://doi.org/10.1007/s11663-015-0343-9
75. Srikanth S, Devi V L, and Kumar R, *Hydrometallurgy* **165** (2016) 125. https://doi.org/10.1016/j.hydromet.2015.09.024
76. Kaminsky Y D, Lyakhov N Z, and Kopylov N I, On high temperature leaching of wolframite. in *Nonferrous Extr Metall New Millenn*, (eds) Rao P R, Kumar R K, Srikanth S, and Goswami N G, National Metallurgical Laboratory, Jamshedpur (1999), p 21.
77. Kumar R, Alex TC, Khan ZH, et al (2005) Mechanical activation of bauxite - Potential and prospects in the Bayer process. In: Kvande H (ed) Light Met. 2005. The Minerals, Metals and Materials Society, Warrendale, pp 77–79